# Emergence of superfluid transport in a dynamical system of ultra-cold atoms

J. Brand[1,2,a] and A.R. Kolovsky[1,3]

[1] Max Planck Institute for the Physics of Complex Systems, Nöthnitzer Straße 38, 01187 Dresden, Germany
[2] Centre of Theoretical Chemistry and Physics, Institute of Fundamental Sciences, Massey University, Auckland, New Zealand
[3] Kirensky Institute of Physics, 660036 Krasnoyarsk, Russia

**Abstract.** The dynamics of a Bose-Einstein condensate is studied theoretically in a combined periodic plus harmonic external potential. Different dynamical regimes of stable and unstable collective dipole and Bloch oscillations are analysed in terms of a quantum mechanical pendulum model. Nonlinear interactions are shown to counteract quantum-mechanical dephasing and lead to phase-coherent, superfluid transport.

**PACS.** 03.75.Lm Tunnelling, Josephson effect, Bose-Einstein condensates in periodic potentials, solitons, vortices and topological excitations – 05.45.-a Nonlinear dynamics and chaos

## 1 Introduction

The study of transport properties of ultra-cold atoms in corrugated potentials has become an intensely discussed topic since the first experiments with Bose-Einstein condensates (BECs) in optical lattices almost a decade ago [1–16]. The observed or predicted phenomena are often discussed by concepts borrowed from the phenomenology of extended systems. This approach led to the characterisation of superfluid and insulating phases and phase transitions [4,13], modulational instability [15,16], and dissipative behaviour [3,14]. However, different dynamical regimes like small-amplitude oscillations, dephasing instabilities, and Bloch oscillations require different models and analogies for their explanation.

In this work we approach the problem from a different, somewhat *holistic* point of view and treat the BEC in the external potential as a finite dynamical system. By mapping this problem onto a simple pendulum model, we are able to explain different dynamical regimes as well as stabilisation and destabilisation mechanisms in a unified approach. Specifically, we consider a cloud of ultra-cold bosonic atoms in a one-dimensional (1D) optical lattice with additional harmonic trapping in the lattice axis. We further confine the analysis to the situation of a sufficiently large number of atoms per site that quantum fluctuations may be neglected. Typical experiments with hundreds of atoms on the central site certainly satisfy this condition but probably the theory still remains valid with much lower atom numbers. This system has been discussed before in many experimental and theoretical works. A dy-

namical "superfluid-insulator" transition has been predicted in reference [5] for a BEC on the basis of a modulational instability caused by nonlinear interactions. A similar effect of insulating behaviour, however, was observed in noninteracting fermions [9]. The latter was interpreted as a very different mechanism in terms of a semiclassical pendulum model. Experiments with BECs [6,7] and further numerical analysis [17,18] gave ambiguous results in showing reduced mobility of bosons without revealing the mechanism.

In this paper we study the BEC in a combined harmonic and lattice trap by exploiting a mapping of this system to a quantum mechanical pendulum model. This exact mapping of the lattice dynamics of the noninteracting system to a simple quantum pendulum model establishes two effects: A separatrix in the semiclassical phase space leads to two separate regions of qualitatively different dynamics (see Fig. 1 and discussion in Sect. 2). Furthermore, dephasing occurs due to quantum-mechanical wave packet motion. Adding non-linear interactions introduces two additional effects: far away from the separatrix, the nonlinearity counteracts the quantum dephasing of the linear problem and thus stabilises wave packet motion. We understand the emerging coherent wave-packet dynamics as a signature of superfluid transport in the sense discussed in the recent literature (see, e.g. Refs. [5,6,10,11]). Close to the separatrix and depending on the strength of the nonlinearity, a dynamical instability destroys coherent wave packet motion. We thus obtain a unified view of such different phenomena as dynamical instability, dephasing, and superfluidity. While a dynamical instability has been predicted by a different mechanism in reference [5] and the effect of the separatrix has been discussed in conjunction

[a] e-mail: J.Brand@massey.ac.nz

with fermions in reference [9], we believe that quantum dephasing and its suppression by nonlinear interactions has not been discussed before [19]. In addition to the stabilisation of dipole oscillations, we also predict a so far undescribed regime of coherent wave packet motion above the separatrix. This regime could be exploited to generate the recently proposed atomic gas at negative kinetic temperatures [20].

## 2 Non-interacting atoms

We begin with dynamics of non-interacting atoms, governed by the Schrödinger equation with the following single-particle Hamiltonian

$$\widehat{H} = \frac{\hat{p}^2}{2M} - V_0 \cos^2\left(\frac{2\pi}{d}x\right) + \frac{M\omega^2}{2}x^2. \tag{1}$$

In equation (1) $M$ is the atomic mass, $V_0$ the depth of the optical potential, $d$ the lattice period, and $\omega$ the frequency of the harmonic confinement. If the lattice potential is large compared to the recoil energy $E_R = 2\hbar^2\pi^2/d^2M$, we may use the tight-binding ansatz for the Schrödinger equation, $\psi(x,t) = \sum_l a_l(t)\psi_l(x)$, where $\psi_l(x)$ are the localised Wannier states. This leads to a system of coupled linear equations for the complex amplitude $a_l(t)$,

$$i\hbar\dot{a}_l = \frac{\nu}{2}l^2 a_l - \frac{J}{2}(a_{l+1} + a_{l-1}), \tag{2}$$

where $\nu = M\omega^2 d^2$ and $J$ is the hopping matrix element, uniquely defined by the depth of the optical lattice $s = V_0/E_R$ as $J/E_R \sim s^{3/4}\exp(-2\sqrt{s})/\sqrt{\pi}$.

A particularly transparent description of the dynamics governed by equation (2) is obtained by mapping it to the mathematical pendulum [22]. Indeed, introducing the function $\phi(\theta,t) = 1/\sqrt{2\pi}\sum_l a_l(t)\exp(il\theta)$, the system of equation (2) reduces to the Schrödinger equation for the quantum pendulum with the Hamiltonian

$$\widehat{H} = \frac{\nu}{2}\widehat{L}^2 - J\cos(\theta), \quad \widehat{L} = -i\frac{\partial}{\partial\theta}. \tag{3}$$

This problem is related to the Mathieu equation [23–26], which is solved by well-known special functions [27]. The full advantage of the representation (3), however, is the easily accessible interpretation in terms of pendulum dynamics. A characteristic feature of the classical pendulum is the existence of a particular trajectory — the separatrix, which separates the vibrational and rotational regimes of the pendulum, see Figure 1. The notion of the separatrix can be well extended into the quantum problem [28]. It is associated with the critical angular momentum, or the critical site index of the original problem,

$$l^* = 2(J/\nu)^{1/2}. \tag{4}$$

The existence of a critical $l^*$ has been indicated in laboratory experiments [6], where the authors excite the system by suddenly shifting the harmonic trap by a distance $\Delta x$. Then, for $l_0 = \Delta x/d < l^*$ (for the lattice
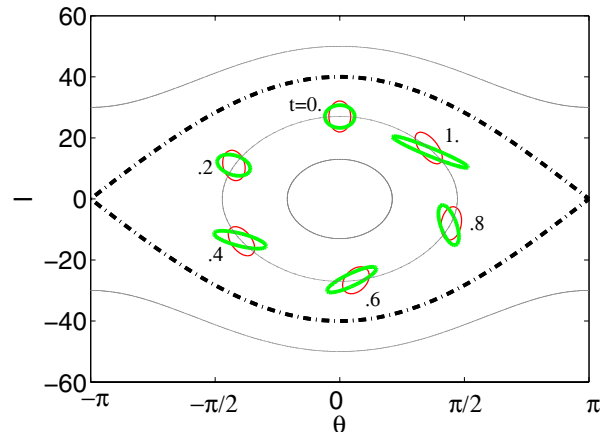


**Fig. 1.** (Color online) Phase space of the classical pendulum in the variables $l$ and $\theta$. The dash-dotted lines show the separatrix for $l^* = 40$, separating rotations from oscillations. These correspond to Bloch and dipole oscillations of a BEC, respectively. Thin (grey) lines indicate classical trajectories with initial conditions $\theta_0 = 0$ and $l_0 = 13, 27, 50, -50$. The quantum time evolution of a Gaussian wave packet is schematised by the 50% contour line of the corresponding Wigner function [21]. After initial displacement from equilibrium position to $l_0 = 27$, $\theta_0 = 0$, solutions of equations (10) are shown in anti-clockwise order for the quantum pendulum at $g = 0$ (thick green contours) and the interacting case at $g/J = 1$ (thin red contours) at times as indicated.

parameters used in the cited experiment $l^* = 134$) the wave packet oscillates around the trap origin, while for $l_0 > l^*$ it sticks to one side of the parabolic potential and the centre-of-mass position can never reach the equilibrium position. For $g = 0$ these dynamical regimes are illustrated in Figure 2. The characteristic frequency of the wave-packet oscillation is given by the pendulum frequency $\Omega(l)$ [29]. Below the separatrix ($l \ll l^*$) we have $\Omega(l) \approx \Omega_0 \equiv (\nu J)^{1/2}/\hbar = \omega(M/M^*)^{1/2}$, where $M^*$ is the effective mass of an atom in the lowest Bloch band. At the separatrix $\Omega(l^*) = 0$ and above ($l \gg l^*$) we have $\Omega(l) \approx \nu l/\hbar$. Note that the dynamics of the atoms for $l > l^*$ can be viewed as Bloch oscillations of the atoms in a (local) static field $F = \nu l_0/d$ with the Bloch frequency $\Omega_{\mathrm{BO}} = dF/\hbar$.

In addition to the effect of the separatrix one can also see the effect of dephasing in Figure 2, which smears out the oscillations of the wave packet as time goes on. This can be related to the non-equidistant spectrum of the quantum pendulum, which is inherited from the nonlinear frequency dependence $\Omega(l)$ of the classical pendulum. If $l^* \gg 1$, a short-time description of the dephasing can be obtained by solving the equations of motion of the classical pendulum for an *ensemble of trajectories* with initial conditions scattered over the phase volume $\sim 2\pi\hbar_{\mathrm{eff}}$ with $\hbar_{\mathrm{eff}} = (\nu/J)^{1/2} = 2/l^*$. As a result we obtain a $t^2$-exponential decay for the oscillations of the mean coordinate and momentum of the atoms. The dephasing is
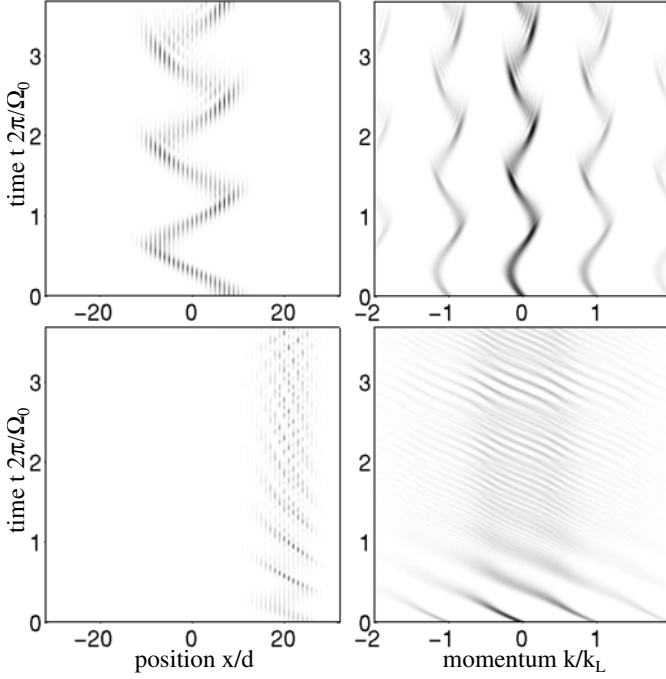
**Fig. 2.** Dynamics of non-interacting atoms ($g = 0$). Gray scale images show the time evolution of the squared wave function after the ground state of the system has been suddenly displaced by the distance $\Delta x$ at $t = 0$. The left and right columns show real space and momentum space plots, respectively, for $\Delta x/d = 8$ (dipole oscillations) in the upper row and for $\Delta x/d = 24$ (Bloch oscillations) in the lower row. The lattice parameters correspond to $J = 2.4 \times 10^{-2} E_R$, $\nu = 3.2 \times 10^{-4} E_R$ (hence, $l^* = 17$). The time axis is scaled by the period $2\pi/\Omega_0$ of small-amplitude pendulum oscillations. Momentum is scaled by the reciprocal lattice constant $k_L = 2\pi/d$. The multiple peak structure of the momentum-space plots is due to the presence of a periodic potential.

conveniently quantified in terms of the quantity

$$\Psi = \sum_l a_l a_{l+1}^*, \qquad (5)$$

which has been introduced as an "order parameter" in reference [5]. In fact, due to the normalisation condition $\sum_l a_l a_l^* = 1$, we find $\Psi \approx 1$ when the site-to-site phase fluctuations are small and $\Psi \approx 0$ in the presence of strong phase fluctuations. The upper left panel of Figure 4 shows the decay of $\Psi$ during dipole oscillations due to dephasing.

Concluding this section we note that the calculations were done by using the continuous nonlinear Schrödinger equation with a lattice depth of $s = 12.16$. For this depth of the optical potential and the considered initial displacement, the results obtained within the tight-binding approach (not shown) practically coincide with the depicted ones. The deviation between the solutions appears only for the initial shift $l_0$ larger than $l_{max} \approx \Delta/\nu$, where $\Delta$ is the energy gap between the ground and first excited Bloch bands. If $l_0 > l_{max}$ the Landau-Zener tunnelling takes place and the single-particle dynamics of the atoms is a superposition of the Bloch and dipole oscillations [30].
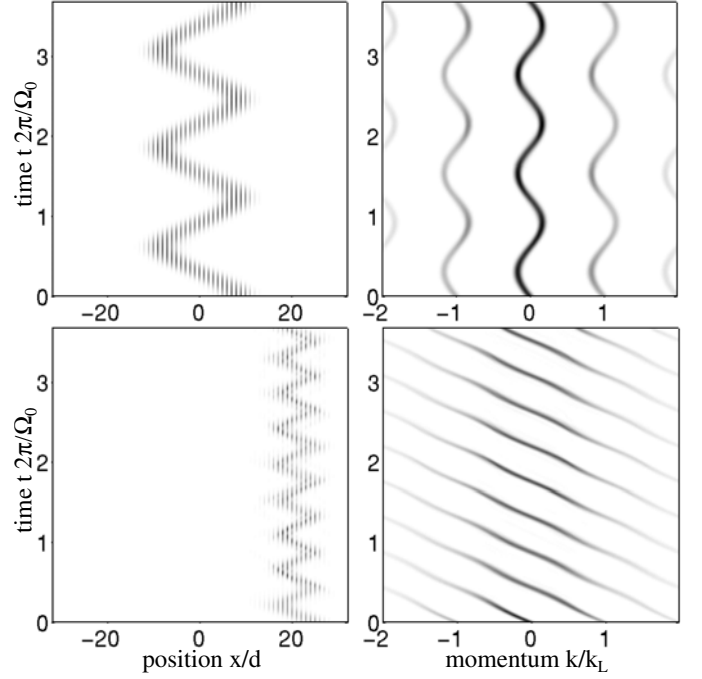
**Fig. 3.** The same as in Figure 2 but for finite nonlinearity $g = 1.55 \times 10^{-2} E_R$.

## 3 Interacting atoms

We shall analyse the case of interacting atoms in the frame of the 1D Gross-Pitaevskii equation,

$$i\hbar \frac{\partial \psi(x,t)}{\partial t} = \widehat{H} \psi(x,t) + g_{1D} |\psi(x,t)|^2 \psi(x,t), \qquad (6)$$

where $g_{1D} \sim a_s \hbar \omega_\perp N$, $a_s$ is the $s$-wave scattering length, $\omega_\perp$ the radial frequency and $N$ the total number of atoms. The tight-binding version of (6) reads as

$$i\hbar \dot{a}_l = \frac{\nu}{2} l^2 a_l - \frac{J}{2} (a_{l+1} + a_{l-1}) + g|a_l|^2 a_l, \qquad (7)$$

where $g = g_{1D} \int |\psi_l(x)|^4 dx \sim a_s \hbar \omega_\perp N/d$.

The main result we want to report in this work is that a weak nonlinearity can compensate the dephasing and the wave packet follows the classical trajectory of the pendulum without dispersion. This is illustrated in Figure 3 and the right column of Figure 4.

### 3.1 Variational approach

In order to estimate the amount of nonlinearity required to convert the quantum dynamics of the pendulum into the 'classical dynamics', we use the Gaussian variational ansatz of reference [31]. For the quantum pendulum this amounts to a semiclassical approximation that can account for dephasing [32]. In this approach, the wave packet
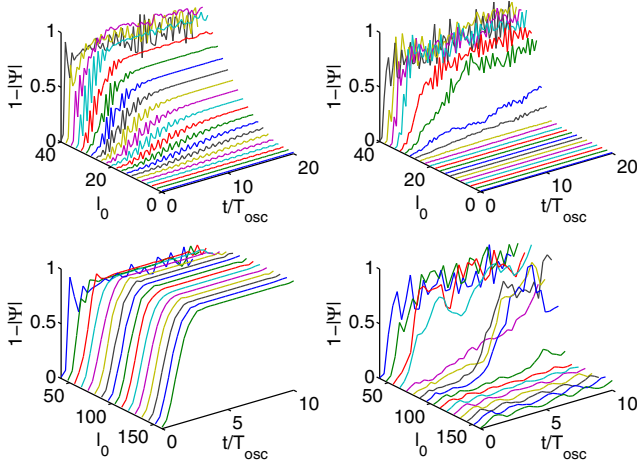
**Fig. 4.** (Color online) Decay of the order parameter $\Psi$ over time for different initial displacements $l_0$ below $l^* = 40$ (upper panels) and above $l^*$ (lower panels). The panels on the left hand side correspond to the noninteracting case ($g = 0$) and the panels on the right to $g/J = 1$.

is parametrised as

$$a_l(t) = \sqrt{A}\exp\left[-\frac{(l-L)^2}{\gamma^2} + i\theta(l-L) + i\frac{\delta}{2}(l-L)^2\right],$$
(8)

where $A$ is a normalisation constant. Then the centre of the wave packet $L(t)$, the dispersion $\gamma(t)$, the velocity $\theta(t)$, and the dephasing parameter $\delta(t)$ satisfy Hamilton's equations for the effective Hamiltonian

$$H_{\text{eff}} = \frac{\nu}{2}\left(L^2 + \frac{\gamma^2}{4}\right) - J\cos\theta e^{-\eta} + \frac{g}{2\sqrt{\pi}\gamma},$$
(9)

where $\eta = 1/2\gamma^2 + \gamma^2\delta^2/8$ and the pairs of canonical variables are $(L,\theta)$ and $(\gamma^2/8,\delta)$, respectively. Thus we have

$$\hbar\dot{L} = -J\sin\theta e^{-\eta}, \quad \hbar\dot{\theta} = \nu L, \quad \hbar\dot{\gamma} = J\gamma\delta\cos\theta e^{-\eta},$$

$$\hbar\dot{\delta} = J\cos\theta\left(\frac{4}{\gamma^4} - \delta^2\right)e^{-\eta} + \frac{2g}{\sqrt{\pi}\gamma^3} - \nu.$$
(10)

The non-dispersive dynamics of the wave packet depicted in the lower row of Figure 2 implies the (quasi)periodic dynamics of the variables $L$, $\theta$, $\gamma$ and $\delta$. In fact, for the certain range of the nonlinearity $g$ and harmonic confinement $\nu$, there is a stable periodic orbit in the four-dimensional phase space of the system (9), which comes through the point $\delta = 0$. The condition for the existence of this periodic orbit is approximately given by the condition

$$g/\nu = \sqrt{\pi}\gamma^3/2,$$
(11)

which means that the last two terms in the equation for $\delta$ cancel each other. Examples of the discussed stable periodic orbits are shown in in the upper two panels of Figure 5. In lower panels of Figure 5 we plot the stability regions of the orbit together with the estimate (11). The bright regions correspond to the quasiperiodic dynamics
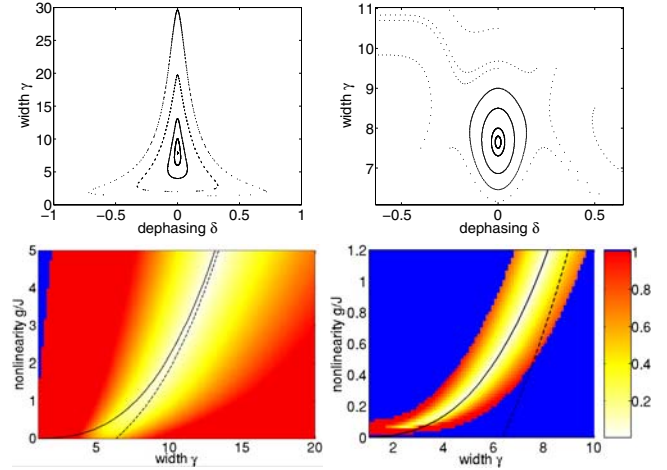


**Fig. 5.** (Color online) Upper panels: Poincaré cross section of the effective system (9) for $l^* = 40$ in the oscillating regime with $l_0 = l^*/2$ (left) and the rotating regime with $l_0 = 4l^*$ (right). The periodic orbit is located in the centre of the stability island. Lower panels: the stability region of the depicted periodic orbit in the $(\gamma, g)$–plane. The relative deviation $\overline{\Delta\gamma/\overline{\gamma}}$ of the width $\gamma$ averaged over the trajectory is shown in grey scale (according to the colorbar). Additionally, the solid line indicates the balance equation (11) and the broken line shows the equilibrium width of the ground state BEC in the given potential.

with small deviations of $\delta$ and $\gamma$. In the grey (red) regions the deviations are large and in the dark (blue) regions the dephasing $\delta$ increases without bounds. It is worth noting that the variational ansatz (8) becomes invalid as soon as the orbit is unbounded or badly bounded. On the other hand, if $\delta(t)$ is captured around $\delta = 0$ and $\gamma$ is not too small as it occurs near the centre of the stability island, we have $\exp[-\eta(t)] \approx 1$ and equation (10) reduces to the equation of motion for a classical pendulum.

Let us estimate the minimum strength of nonlinearity needed in order to suppress dephasing. A coarse estimate may be obtained by the requirement that the equilibrium width of the wave packet is compatible with equation (11). The minimum value $g_{\min}$ can be found by requiring that the width $\gamma$ obtained from equation (11) is equal to the non-interacting equilibrium width. We obtain the condition

$$g \geq \frac{\sqrt{\pi}\nu^{7/4}}{2^{5/2}J^{3/4}} \approx 0.31\left(\frac{\nu^7}{J^3}\right)^{1/4}.$$
(12)

## 3.2 Numerical results

The above approach to the wave packet dynamics, which is based on the effective Hamiltonian (9), may be still oversimplified. For this reason and in order to check the estimate (12) we run the DNLS for different values of the nonlinearity $g$ and harmonic confinement $\nu$. In order to reduce the number of independent parameters we have also assumed that the shape of the initial wave packet is

defined by the ground state of the BEC before shifting the trap centre and, hence, the wave packet width $\gamma$ is no more an independent parameter (see the dashed line in the stability diagrams in Fig. 5). The results of these numerical studies can be summarised as follows:

(i)   the effect of stabilisation is sensitive to the initial shift of the packet $l_0$ relative to the position of the separatrix (4). In particular, no stabilisation was observed for $l_0 \approx l^*$. This is actually not surprising — the separatrix is the most fragile trajectory of the pendulum and any tiny perturbation destroys it;

(ii)   if $l_0$ is sufficiently far away from the separatrix, there is a finite interval of nonlinearity $g_{\min} < g < g_{\max}$ where the BEC oscillations are not decaying;

(iii)   the lower boundary $g_{\min}$ is defined by the condition for appearance of a (non-negligible) stability island for the effective system (8) and is approximately given by equation (12);

(iv)   the upper boundary $g_{\max}$ strongly depends on $l_0$ and sometimes is not well defined in the sense that for a large $g$ we find a transient or incomplete stabilisation. An example is seen in the lower right panel of Figure 4 in the rapid increase of $1 - |\psi|$ for initial values near $l_0 \approx 80$. This result (taken together with the existence of the stability island) suggests, that along with the stabilisation, the nonlinearity induces a different process in the system which destroys the regular oscillations of the condensate when $g$ exceeds some critical value. A more sophisticated approach than the variational ansatz (8) is required to take this effect into account.

A boundary for the stability of dipole oscillations was proposed before in reference [5] by a simple argument based on the modulational instability of plane wave states. This argument lead to a critical value of $l^*/\sqrt{2}$ for the initial displacement. Our numerical calculations loosely support this estimate for $g/J \approx 1$ (see the upper right panel in Fig. 4) but also show additional dependence on $g/J$ and $l^*$ as well as significant deviations in other parameter regimes.

It is important to realize, however, that instable motion below the separatrix (for $l_0 < l^*$) and the associated dephasing leads to a mean position of the wave packet at the equilibrium position of the harmonic potential whereas the stable or unstable motion above the separatrix (for $l_0 > l^*$) is characterised by a nonzero offset from the equilibrium position. Hence both effects have very different character.

### 3.3 Relation to Bloch oscillations of homogeneous BEC

At this point we briefly mention the related problem of the dynamical (modulational) instability that has been studied in the context of the Bloch oscillations of a BEC subjected to a static force $F$. In this case the mean-field
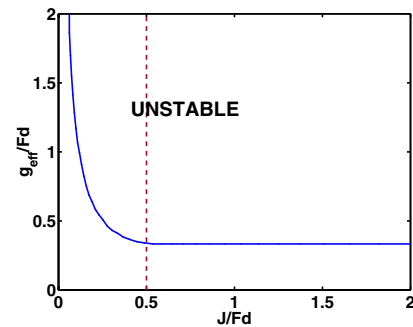


**Fig. 6.** Stability diagram for Bloch oscillations in a homogeneous system. Here, $g_{\mathrm{eff}} = gN/L$ is an effective coupling constant. The dashed line separates the "universal" regime of weak forcing, where $g_{cr} = 3.0Fd$, from the "non-universal" regime of strong forcing, where $g_{cr}$ additionally depends on $J$.

equation corresponding to equation (7) reads

$$i\hbar\dot{a}_l = -\frac{J}{2}\left(a_{l+1} + a_{l-1}\right) + g|a_l|^2 a_l + Fd\,l\,a_l, \qquad (13)$$

where $d$ is the lattice constant and the initial particle number density $|a_l|^2 = N/L$ is assumed to be constant and large compared to one; $N$ and $L$ are the number of particles and system size, respectively. Time-periodic solutions of equation (13) correspond to Bloch oscillations and generalise the Bloch oscillations known from non-interacting particles in periodic potentials. As shown in the recent papers [33,34], there is a critical value of the nonlinearity, below which these Bloch oscillations are stable, while above they are subject to a dynamical instability. This instability scrambles the relative phases and leads to inhomogeneous, time-aperiodic density distributions. The stability diagram of Figure 6 summarises the results.

Since the dynamics of the atoms in a parabolic lattice for $l_0 \gg l^*$ can be alternatively viewed as Bloch oscillations in a static field with the local magnitude $F = \nu l_0/d$, a rough estimate for the expected instability regime may be drawn from this critical nonlinearity. However, an important difference between the two systems is that the modulational instability analysis assumes a uniform state $\gamma \to \infty$, while in the pendulum dynamics the finiteness of $\gamma$ is a crucial ingredient. Indeed, numerical explorations indicate that the parameter dependence is more complicated, which makes this an interesting problem for further study.

### 3.4 Relation to superfluidity

The concept of superfluidity rest on a rich phenomenology rather than precise definitions [35]. As mentioned above, we associate the emergence and breakdown of coherent dynamics with superfluidity in this paper in alignment with discussions in the recent literature related to cold atom experiments. In contrast to the traditional approach from condensed matter theory considering infinite systems in the thermodynamic limit, we are dealing here with an

intrinsically finite dynamical system for which the concept of superfluidity yet has to be defined.

Clearly, a mere application of concepts borrowed from the theory of infinite systems will not help here: as an example we mention the Landau critical velocity, which is bounded from above by the speed of sound $v_s$, which is a function of the density. In a local-density-type argument, we may consider the variation of the density over the wave packet and conclude that the critical velocity for the breakdown of superfluidity should vanish, as $v_s \rightarrow 0$ in the tails of the wave packet. Thus, we would not expect superfluid transport even though we implicitly assume that the atoms are completely Bose condensed by using equation (6). Nevertheless, we predict coherent transport in certain parameter regimes as discussed above.

A systematic study of the robustness of the superfluid behaviour against energy dissipation from small impurities is beyond the scope of the current paper but will constitute an interesting extension of the present work.

## 4 Conclusions

In conclusion, we have considered the 1D dynamics of a BEC of cold atoms in parabolic optical lattices. When interactions are absent, this system realizes the quantum pendulum (3) with the experimentally controllable effective Planck constant $\hbar_{\text{eff}} = 2/l^*$, where $l^*$ of equation (4) characterises the pendulum separatrix. The parameter $l^*$ plays an important role both in theory and experiment. In particular, the relation between $l^*$ and the trap centre shift $l_0 = \Delta x/d$, used in the experiments to put the atoms in motion, defines whether BEC oscillations are symmetric with respect to the trap origin or not. The parameter $\hbar_{\text{eff}} = 2/l^*$ also defines the rate of dephasing, because of which BEC oscillations decay even in the absence of atom-atom interactions. The effect of the latter on the discussed dynamics appears to be nontrivial. Naively, one would expect that any nonzero interaction enhances the decay of BEC oscillations. However, this is not the case – a moderate nonlinearity is found to stabilise the oscillations, which now can be described in terms of the *classical* pendulum. The emergence of superfluid behaviour is thus related to a quantum-classical transition. We believe that for $l_0 < l^*$ the stable regime of wave packet dynamics has been actually realized in the experiment [6], where periodic oscillations of a BEC with a frequency given by the frequency of the classical pendulum have been observed and interpreted as a superfluid phenomenon. In order to see the transition to dephasing-dominated dynamics, the experiments would have to work at lower particle number densities or reduce the nonlinear coupling constant, e.g. with $^7$Li atoms [36], by tuning the atomic scattering length by means of a magnetic Feshbach resonance. Most surprisingly, stabilisation of wave packet motion may also occur above the separatrix, which appears to not have been observed yet.

## References

1. B.P. Anderson, M.A. Kasevich, Science **282**, 1686 (1998)
2. F.S. Cataliotti et al., Science **293**, 843 (2001)
3. S. Burger et al., Phys. Rev. Lett. **86**, 4447 (2001)
4. M. Greiner et al., Nature **415**, 39 (2002)
5. A. Smerzi, A. Trombettoni, P.G. Kevrekidis, A.R. Bishop, Phys. Rev. Lett. **89**, 170402 (2002)
6. F.S. Cataliotti et al., New J. Phys. **5**, 71 (2003)
7. F.S. Cataliotti et al., J. Opt. B **5**, S17 (2003)
8. G. Orso, L.P. Pitaevskii, S. Stringari, Phys. Rev. Lett. **93**, 020404 (2004)
9. L. Pezze et al., Phys. Rev. Lett. **93**, 120401 (2004)
10. H. Ott et al., Phys. Rev. Lett. **92**, 160601 (2004)
11. C.D. Fertig et al., Phys. Rev. Lett. **94**, 120403 (2005)
12. A.M. Rey, G. Pupillo, C.W. Clark, C.J. Williams, Phys. Rev. A **72**, 033616 (2005)
13. E. Altman et al., Phys. Rev. Lett. **95**, 020402 (2005)
14. A. Polkovnikov et al., Phys. Rev. A **71**, 063613 (2005)
15. B. Wu, Q. Niu, New J. Phys. **5**, 104 (2003)
16. V.V. Konotop, M. Salerno, Phys. Rev. A **65**, 021602(R) (2002)
17. S. Adhikari, Eur. Phys. J. D **25**, 161 (2003)
18. F. Nesi, M. Modugno, J. Phys. B **37**, S101 (2004)
19. Dephasing in the weakly-interacting limit was first discussed in a previous version of this paper, `arXiv:cond-mat/0412549v1` (2004), and later was mentioned in reference [12]
20. A.P. Mosk, Phys. Rev. Lett. **95**, 040403 (2005)
21. W.P. Schleich, *Quantum Optics in Phase Space* (Wiley-VCH, Berlin, 2001)
22. A.R. Kolovsky, H.J. Korsch, Int. J. Mod. Phys. **18**, 1235 (2004)
23. D.C. Mattis, Rev. Mod. Phys. **58**, 361 (1986)
24. C. Hooley, J. Quintanilla, Phys. Rev. Lett. **93**, 080404 (2004)
25. M. Rigol, A. Muramatsu, Phys. Rev. A **70**, 043627 (2004)
26. V. Ruuska, P. Törmä, New J. Phys. **6**, 59 (2004)
27. *Handbook of Mathematical Functions*, edited by A. Abramowitz, I. Stegun (Dover, New York, 1972)
28. G.P. Berman, G.M. Zaslavskii, A.R. Kolovskii, Sov. Phys. JETP **54**, 272 (1981)
29. A.J. Lichtenberg, M.A. Libermann, *Regular and chaotic dynamics* (Springer, Berlin, 1983)
30. A.V. Ponomarev, A.R. Kolovsky, A. Buchleitner, to be published
31. A. Trombettoni, A. Smerzi, Phys. Rev. Lett. **86**, 2353 (2001)
32. E.J. Heller, J. Chem. Phys. **62**, 1544 (1975)
33. Y. Zheng, M. Kostrun, J. Javanainen, Phys. Rev. Lett. **93**, 230401 (2004)
34. A.R. Kolovsky, `arXiv:cond-mat/0412195`
35. A.J. Leggett, Rev. Mod. Phys. **71**, S318 (1999)
36. L. Khaykovich et al., Science **296**, 1290 (2002)